

See discussions, stats, and author profiles for this publication at: <https://www.researchgate.net/publication/233845674>

# Electrical, structural and optical characterization of copper oxide thin films as a function of post annealing temperature

ARTICLE in PHYSICA STATUS SOLIDI (A) · SEPTEMBER 2009

Impact Factor: 1.21 · DOI: 10.1002/pssa.200881797

---

CITATIONS

34

READS

76

---

## 8 AUTHORS, INCLUDING:



Vitor Figueiredo

New University of Lisbon

9 PUBLICATIONS 280 CITATIONS

[SEE PROFILE](#)



Elangovan Elamurugu

Masdar Institute of Science and Technology

78 PUBLICATIONS 1,214 CITATIONS

[SEE PROFILE](#)



R. Martins

Institute for the Development of New Tech...

615 PUBLICATIONS 8,825 CITATIONS

[SEE PROFILE](#)



Elvira Fortunato

New University of Lisbon

609 PUBLICATIONS 9,464 CITATIONS

[SEE PROFILE](#)

# physica status solidi

[www.interscience.wiley.com](http://www.interscience.wiley.com)

**reprints**

The collage consists of five journal covers arranged in a grid-like fashion:

- physica status solidi a**: Applications and materials science. Cover image shows a 3D schematic of a light-emitting diode structure with three arrows labeled  $h\nu$  pointing upwards.
- physica status solidi b**: Basic solid state physics. Cover image shows a 3D plot of electron density in a crystal lattice.
- physica status solidi c**: Current topics in solid state physics. Cover image shows a photograph of a laser experiment with a red beam and a blue inset diagram.
- physica status solidi rrl**: Rapid research letters. Cover image shows a 3D molecular model with a central atom and surrounding ligands.
- REPRINT**: A red diagonal banner across the bottom right corner.

Below each journal cover is its website address:

- [www.pss-a.com](http://www.pss-a.com)
- [www.pss-b.com](http://www.pss-b.com)
- [www.pss-c.com](http://www.pss-c.com)
- [www.pss-rapid.com](http://www.pss-rapid.com)

# Electrical, structural and optical characterization of copper oxide thin films as a function of post annealing temperature

V. Figueiredo<sup>1</sup>, E. Elangovan<sup>1</sup>, G. Gonçalves<sup>1</sup>, N. Franco<sup>2</sup>, E. Alves<sup>2</sup>, S.H.K. Park<sup>3</sup>, R. Martins<sup>1</sup>, and E. Fortunato<sup>\*1</sup>

<sup>1</sup> Materials Science Department, CENIMAT-I3N and CEMOP-UNINOVA, FCT-UNL, Campus da Caparica, 2829-516 Caparica, Portugal

<sup>2</sup> LFI, Dep. Física, Instituto Tecnológico e Nuclear, EN10, 2686-953 Sacavém, Portugal

<sup>3</sup> Basic Research Laboratory, Electronics and Telecommunications Research Institute, Transparent Electronics Team, Yusong-gu, Daejeon 305-350, Korea

Received 26 November 2008, revised 28 January 2009, accepted 26 February 2009

Published online 28 July 2009

PACS 61.05.cp, 68.37.Ps, 72.20.-i, 78.20.Ci, 81.15.Ji

\* Corresponding author: e-mail emf@fct.unl.pt, Phone: +351 212948562 (#11609), Fax: +351 212948558

Copper oxide thin films were obtained by annealing (temperature ranging between 100 and 450 °C) the metallic Cu films deposited on glass substrates by e-beam evaporation. XRD studies confirmed that the cubic Cu phase of the as-deposited films changes into single cubic Cu<sub>2</sub>O phase and single monoclinic CuO phase, depending on the annealing conditions. The crystallite size is varied between ~12 and 31 nm. The lattice parameters of cubic Cu and Cu<sub>2</sub>O phases are estimated to ~3.60 and ~4.26 Å, respectively. The films with Cu<sub>2</sub>O phase showed

p-type characteristics. The conductivity is decreased linearly with the decreasing temperature (1/T), which has confirmed the semiconductor nature of the deposited films. The calculated activation energy is varied between 0.10 and 0.16 eV. The surface microstructure is changed depending on the variation in the annealing temperature. The poor transmittance of the as-deposited films (<1%) is increased to a maximum of ~80% (800 nm) on annealing at 200 °C. The estimated direct allowed band gap is varied between 1.73 and 2.89 eV.

© 2009 WILEY-VCH Verlag GmbH & Co. KGaA, Weinheim

**1 Introduction** The development of p-type semiconductors is one of the key technologies for p-n junction based devices such as diodes, transistors, and light emitting diodes [1]. Copper oxide (CO) is a proven p-type transparent conducting oxide (TCO) semiconductor for fabricating variety of devices. Two common forms of CO are cuprous oxide or cuprite (Cu<sub>2</sub>O) and cupric oxide or tenorite (CuO) [1]. Both the CuO (monoclinic) and Cu<sub>2</sub>O (cubic) are p-type semiconductors with a band gap ranging 1.9–2.1 and 2.1–2.6 eV, respectively [2]. Cu<sub>2</sub>O is one of the oldest semiconducting materials [3] that is used in solar cell applications [4], owing to the fact that the constituent materials are nontoxic and abundantly available on the earth. As a p-type semiconductor, conduction arises from the presence of holes in the valence band (VB) due to doping/annealing [5]. Unlike the other oxides, the top states of VB in Cu<sub>2</sub>O is derived from the fully occupied Cu 3d<sup>10</sup>

states which are not localized (more mobile) when converted into holes [6]. Formation of Cu vacancy is an often stated mechanism for the origin of p-type conductivity in Cu<sub>2</sub>O [5]. Stoichiometric Cu<sub>2</sub>O is a well-studied material and its first principles studies can be found in Ref. [7]. CuO is also an interesting candidate in the applications of solar energy converting devices, gas sensors, and superconducting devices [8]. A variety of deposition techniques such as electro deposition, thermal oxidation, chemical deposition, sputtering, plasma evaporation, sol–gel, molecular beam epitaxy, and chemical vapor deposition [1, 9–16] have been employed to study the CO films. Aiming the development of p-n junction-based oxide devices [17], the research on CO thin films has attracted the researchers globally. The CO films in the present study were obtained through the conventional thermal oxidation of electron (e-) beam evaporated metallic copper (Cu) films. The physical properties of the films were

studied in order to find the possibility to use them in p–n junction-based applications.

**2 Experimental details** Thin films of Cu were deposited on microscopic glass substrates ( $25 \times 25 \times 1 \text{ mm}^3$ ) by e-beam evaporating the Cu pellets (CERAC; 99.999%). The distance between the source and substrate was  $\sim 25 \text{ cm}$ . The thickness of the films measured using profilometry was found to be  $\sim 150 \text{ nm}$ , which is in agreement with the value obtained through quartz crystal monitor mounted in the evaporation unit. The as-deposited Cu films were post-annealed at temperatures ranging  $100\text{--}450^\circ\text{C}$  in open air for 30 min. The thickness of the films is increased to ranging  $\sim 170\text{--}180 \text{ nm}$  on annealing, which is presumably due to the change in crystallinity. The details on the characterization techniques can be found in Ref. [18].

**3 Results and discussion** The XRD patterns confirmed that the as-deposited metallic cubic Cu phase (ICDD File no. 04-0836; space group #225) is partially oxidized to Cu<sub>2</sub>O (ICDD File no. 05-0667; space group #224) at the initial annealing temperature ( $T_a$ ) of  $100^\circ\text{C}$  which results in mixed Cu–Cu<sub>2</sub>O phase. A single Cu<sub>2</sub>O phase was obtained for the  $T_a$  of 200 and  $250^\circ\text{C}$ . A mixed Cu<sub>2</sub>O–CuO phase was obtained for the  $T_a$  of  $300^\circ\text{C}$  similar to that was reported earlier [11]. This mixed phase is then changed to a single CuO phase (ICDD File nos.: 45-0937 & 48-1548; space group #15) for the  $T_a$  between 350 and  $450^\circ\text{C}$ . The conversion of Cu<sub>2</sub>O to CuO during annealing in the presence of oxygen is well known [19]. It is earlier reported by Nair and coworkers [11] that the Cu<sub>2</sub>O phase is converted into CuO phase when annealed at  $350^\circ\text{C}$ , which corroborates the present work. It is also reported that at still higher temperature, CuO could revert to Cu<sub>2</sub>O [19], but however the possibility is not verified in the present work. A more detailed report on the patterns can be found in our earlier report [18]. The data obtained from XRD analysis are quantified in Table 1. The full width half maximum (FWHM) obtained from the diffraction peak of Cu phase is increased from  $\sim 0.28$  to about  $\sim 0.76^\circ$  for the single Cu<sub>2</sub>O at  $T_a$  of  $200^\circ\text{C}$ . This increase in FWHM is suggesting a reduction in crystallite size ( $L$ ). However, the FWHM is decreased gradually with the further increase in  $T_a$  to reach  $\sim 0.41^\circ$  at  $400^\circ\text{C}$ , but then increased slightly ( $450^\circ\text{C}$ ). The  $L$  is calculated using the familiar Scherrer's formula [20] that is given below:

$$L = \frac{0.9\lambda}{\beta \cos \theta}, \quad (1)$$

where  $\lambda$  is the wavelength of the X-rays used,  $\beta$  the full width at half maximum (FWHM) in radians, and  $\theta$  the diffraction angle. The maximum  $L$  of  $\sim 30 \text{ nm}$  obtained for the Cu phase is decreased to about  $\sim 12 \text{ nm}$  when the  $T_a$  is increased to  $200^\circ\text{C}$ . However,  $L$  is gradually increased with the further increase in  $T_a$  (Table 1). The obtained  $L$  values corroborate the changes in FWHM of the deposited films. The variation in  $L$  and FWHM substantiates the change in the crystal structure

**Table 1** XRD data of the CO films as a function of annealing temperature (symbol representations: # – metallic Cu phase, ▲ – Cu<sub>2</sub>O phase and △ – CuO phase)

$T_a$ (°C)	phase	$hkl$	$2\theta$ (°)	FWHM (°)	crystallite size (nm)
RT	Cu	(111) <sup>#</sup>	43.37	0.271	30.78
		(200) <sup>#</sup>	50.70	—	—
100	Cu	(111) <sup>#</sup>	43.37	0.284	29.37
		(200) <sup>#</sup>	50.70	—	—
200	Cu <sub>2</sub> O	(111) <sup>▲</sup>	36.56	—	—
		(111) <sup>▲</sup>	36.56	0.764	12.36
250	Cu <sub>2</sub> O	(111) <sup>▲</sup>	36.56	0.573	16.48
		(111) <sup>▲</sup>	36.56	—	—
300	Cu <sub>2</sub> O	(111) <sup>▲</sup>	36.56	—	—
		CuO	(11̄1) <sup>△</sup>	35.70	—
350	CuO	(11̄1) <sup>△</sup>	35.70	—	—
		(111) <sup>△</sup>	38.73	0.523	17.48
400	CuO	(11̄1) <sup>△</sup>	35.70	—	—
		(111) <sup>△</sup>	38.73	0.411	22.24
450	CuO	(11̄1) <sup>△</sup>	35.70	—	—
		(111) <sup>△</sup>	38.73	0.460	19.87

FWHM – full width at half maximum.

of the films as mentioned above. The lattice parameter ( $a$ ) of cubic phase (Cu and Cu<sub>2</sub>O) is estimated using the equation found in Ref. [20]:

$$\frac{h^2 + k^2 + l^2}{a^2} = \frac{4 \sin^2 \theta}{\lambda^2}. \quad (2)$$

The values of  $h$ ,  $k$ , and  $l$  are obtained from the diffraction peak;  $\theta$  is the diffraction angle;  $\lambda$  is the wavelength (1.5419 Å) of the X-rays used for diffraction. With the available values, the equation is solved to estimate  $a$ . The calculated  $a$  is 3.60 Å for the films with Cu phase (as-deposited and the films annealed at  $100^\circ\text{C}$ ). A value of 4.26 Å is obtained for the films with Cu<sub>2</sub>O phase. The increase in  $a$  also authenticate the variation in the structural properties of the films as a function of  $T_a$ .

The surface microstructure of the films was analyzed by AFM. The typical AFM microstructures obtained from the surface of the as-deposited and post-annealed films are shown in Fig. 1. The surface of as-deposited films is comprised of uniformly distributed and well-packed grains ranging  $\sim 10\text{--}20 \text{ nm}$  in size, with a RMS roughness of  $\sim 1.47 \text{ nm}$ . However, there appear few bigger grains with the size as big as  $\sim 40 \text{ nm}$ . For  $T_a$  of  $100^\circ\text{C}$ , the surface show randomly distributed cluster of grains, which has presumably increased the RMS roughness to  $\sim 11.78 \text{ nm}$ . The size of the grains vary between  $\sim 10$  and  $30 \text{ nm}$  with few agglomerated grains as big as  $\sim 60 \text{ nm}$  on top of smaller grains. There appear few drains throughout the surface of the films. The drains seem to contain grains underneath that are not distinguishable presumably due to the technical

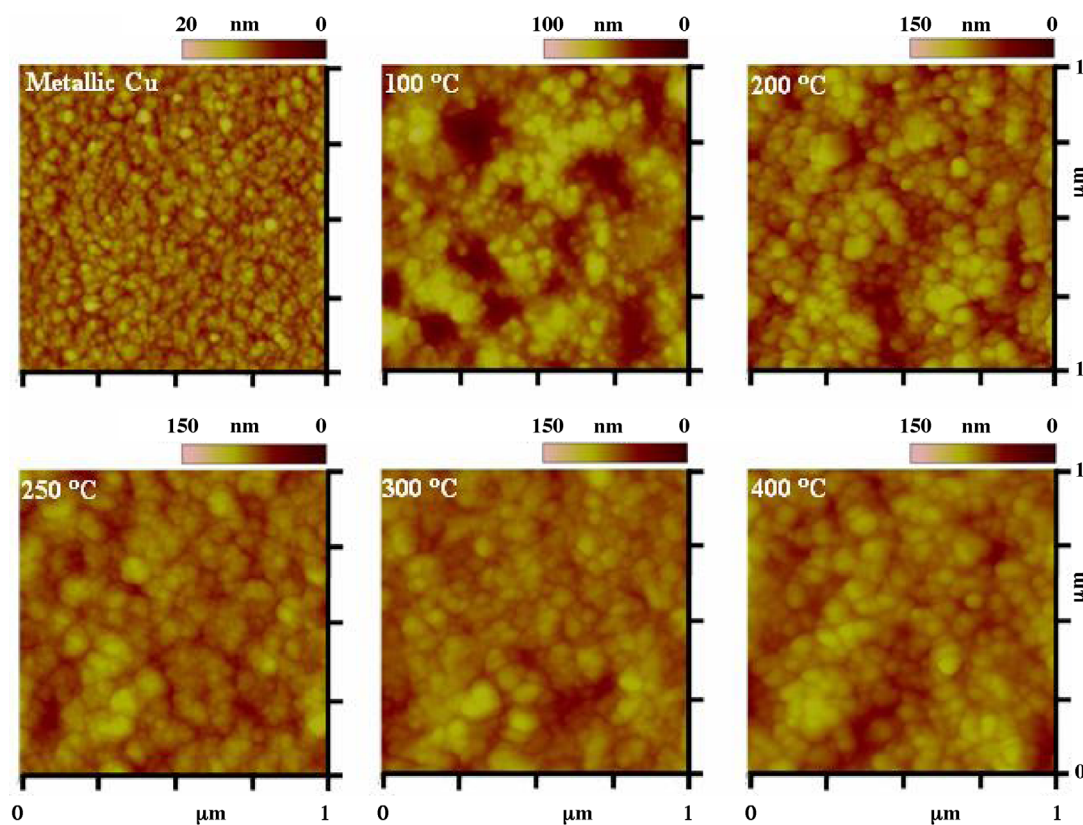


**Figure 1** (online color at: [www.pss-a.com](http://www.pss-a.com)) AFM microstructures of the CO films as a function of annealing temperature.

limitation of AFM. The RMS roughness is found to increase to a maximum of  $\sim 14.42$  nm on annealing at  $200^\circ\text{C}$  but then decreased gradually to  $\sim 10.26$  nm when annealed at  $450^\circ\text{C}$ . The variation in the microstructure and the roughness corroborates the structural studies. The drains are suppressed for the  $250^\circ\text{C}$  annealing, which is probably suggesting that the grains are distributed uniformly due to the increased surface energy. The grains are cubical in shape and their sizes vary between  $\sim 15$  and  $30$  nm. The grains are held together by the uniformly distributed bunches, which gives a cauliflower-like morphology. There appear agglomerated grains as big as  $\sim 70$  nm on top of this morphology. The size of the grains increases to a range of  $\sim 20$ – $40$  nm when the films are annealed at  $>300^\circ\text{C}$ , with fewer agglomerated grains on the surface.

The variation in electrical parameters (Hall measurements) is shown schematically in Fig. 2a. The type of conductivity is confirmed from the sign of Hall coefficient. The as-deposited and low temperature ( $100^\circ\text{C}$ ) annealed films showed n-type conductivity. The conductivity is changed to p-type for the films annealed between  $200$  and  $300^\circ\text{C}$ , where the  $\text{Cu}_2\text{O}$  phase is dominant. The conductivity is reverted to n-type for the further increase in  $T_a$  ( $>350^\circ\text{C}$ ), where  $\text{CuO}$  phase is dominant. The variation in type of conductivity thus reveals that the films are p-type conducting

when the films crystallize in  $\text{Cu}_2\text{O}$  phase. For the CO films, the change in type of conductivity has been reported earlier with annealing temperature and consequently with composition of the films [10]. It is known that the electrical transport properties are dependent on the composition and crystalline structure of the prepared films. The films reported in the present study undergo the change in the crystalline structure from  $\text{Cu}_2\text{O}$  phase to  $\text{CuO}$  depending on the annealing temperature as mentioned before. This change in the crystalline structure may have presumably varied the electrical transport mechanism of the films to result in the variation of the type of conductivity. However, the change in transport mechanism needs to be studied in detail. The resistivity ( $\rho$ ) of the films annealed at  $100^\circ\text{C}$  is increased from  $2.73 \times 10^{-5}$  to  $5.51 \times 10^2 \Omega \text{ cm}$  for the increase in  $T_a$  to  $300^\circ\text{C}$ . The  $\rho$  is then decreased with the increasing  $T_a$  by an order of magnitude to  $3.1 \times 10^1 \Omega \text{ cm}$  when annealed at  $450^\circ\text{C}$ . The carrier concentration ( $n$ ) of the films annealed at  $100^\circ\text{C}$  (dominating metallic Cu phase) decreased from  $3.75 \times 10^{22} \text{ cm}^{-3}$  by about six orders of magnitude to  $3.69 \times 10^{16} \text{ cm}^{-3}$  when annealed at  $200^\circ\text{C}$ . The  $n$  was then gradually increased with increasing  $T_a$  to reach  $7.19 \times 10^{17} \text{ cm}^{-3}$  at  $450^\circ\text{C}$ . The mobility ( $\mu$ ) of the films annealed at  $100^\circ\text{C}$  is decreased abruptly from  $6.11$  to  $1.56 \text{ cm}^2/\text{V} \cdot \text{s}$  for the increase in  $T_a$  to  $200^\circ\text{C}$ , but

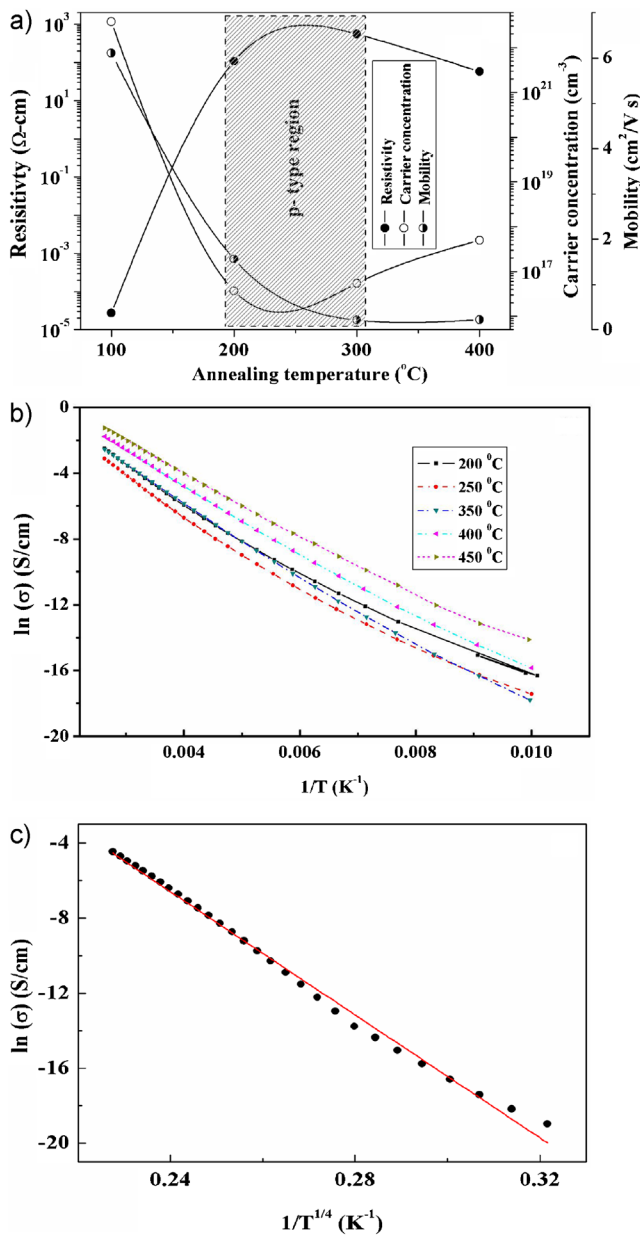


**Figure 2** (online color at: [www.pss-a.com](http://www.pss-a.com)) Electrical properties of the CO thin films: (a) Variation in the Hall parameters, (b) (1/T) vs. conductivity of the annealed films, and (c) ( $1/T^{1/4}$ ) vs. conductivity of the films annealed at 300 °C.

then decreased gradually to  $0.28 \text{ cm}^2/\text{V} \cdot \text{s}$  at 450 °C. The conspicuous aspect of electrical properties is that the films with Cu<sub>2</sub>O show p-type conductivity. However, a relatively poor crystallinity of these films leads to the reduced electrical characteristics.

The dependence of DC conductivity ( $\sigma$ ) was observed in the temperature ( $T$ ) ranging between 100 and 373 K. The variation in  $\ln(\sigma)$  between the post-annealed films is shown in Fig. 2b as a function of  $1/T$ . It is perceptible that  $\sigma$  is decreasing linearly with the increasing value of  $1/T$ , which

confirm the semiconductor nature of the deposited films. Further, the  $\sigma$  of the films annealed at 200 °C is decreased slightly when the  $T_a$  is increased to 250 °C but then decreased significantly for the increase in  $T_a$  to 300 °C. The  $\sigma$  is increased sharply for the increase in  $T_a$  from 300 to 350 °C. However, the increment becomes gradual when the  $T_a$  is increased above 350 °C. It may be noteworthy that a similar kind of variation in  $\rho$  was observed as shown in Fig. 2a, which corroborate the conductivity measurements. The difference in conductivity with the variation in  $T_a$  may be attributed to the change in the crystallinity phase. The activation energy ( $E_A$ ) of the deposited films was estimated using the Arrhenius equation

$$\ln \sigma = \ln \sigma_0 + \frac{-E_A}{k_B T}, \quad (3)$$

where  $\sigma_0$  is the pre-exponential term,  $E_A$  is the activation energy for conduction,  $k_B$  the Boltzmann constant ( $8.617 \times 10^{-5} \text{ eV/K}$ ) and  $T$  is temperature in Kelvin. The obtained  $E_A$  values are varied ranging 0.10–0.16 eV. The obtained values are in agreement with the previous report on CO thin films [21]. It may be noteworthy that the conductivity data obtained from the films annealed at 300 °C cannot fit linearly in comparison with other samples. This situation can be explained if we take into account the existence of two different CO phases (Table 1) in this sample, namely CuO and Cu<sub>2</sub>O. However, electron conduction seems to be described by the variable-range hopping mechanism, described by the equation

$$\sigma = A \exp \left[ - \left( \frac{T_0}{T} \right)^{1/4} \right], \quad (4)$$

where

$$T_0 = \frac{1.5}{\alpha^3 N(E) k_B}, \quad (5)$$

$A$  is a constant,  $\alpha$  the inverse of the radius states, and  $N(E)$  is the density of states at the Fermi level. Hence, for this sample the plot is made using the  $(1/T^{1/4})$  values in the X-axis (Fig. 2c).

The transmittance spectra are shown in Fig. 3a as a function of  $T_a$ . The poor transmittance (<1%) of the as-deposited films (due to absorption of Cu) is increased on annealing, and the transmittance of the films annealed at >200 °C is varying between ~70 and 80%. The average visible transmittance (AVT; wavelength ranging 600–800 nm) is varied between ~5 and 66%. The minimum AVT of ~5% obtained for the films annealed at 100 °C is increased to ~66% at 200 °C. The AVT is decreased to ~50% for the films annealed at 250 °C. However, the films annealed at >300 °C showed an AVT of around 40%. The direct-allowed optical band gap ( $E_g$ ) estimated [22] for the films annealed at temperatures in the range 200–450 °C from the plot (Fig. 3b) is varied between 1.73 and 2.89 eV. All

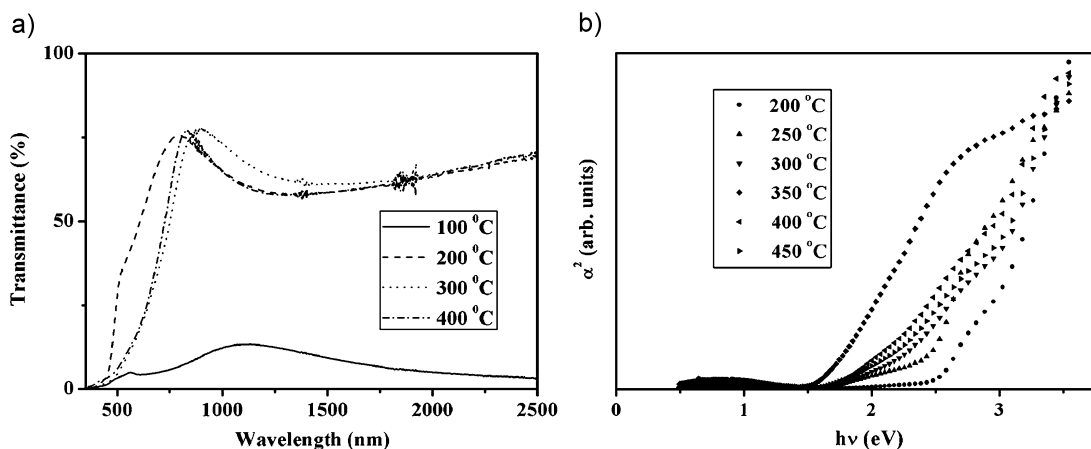


**Figure 3** Comparison of optical properties of the CO films as a function of annealing temperature: (a) Transmittance spectra and (b)  $\alpha^2$  vs.  $h\nu$  plots.

the films annealed at  $> 200^\circ\text{C}$  show dual  $E_g$  values with an exception for those annealed at  $350^\circ\text{C}$ . We have earlier reported a similar kind of behavior for gallium doped zinc oxide films annealed at  $500^\circ\text{C}$  [23]. In general, the presence of dual band gap occurs due to the mixed phase or poor crystallinity [24]. The present situation can be attributed to the relatively poor crystallinity of the films. To the best of authors' knowledge the value of  $2.89\text{ eV}$  obtained in the present study is the highest reported  $E_g$  value for CO thin films. A relatively low  $E_g$  value ( $1.73\text{ eV}$ ) obtained for the films annealed at  $350^\circ\text{C}$  may probably suggest that the films have some structural defects which needs to be studied in detail.

**4 Conclusion** Copper oxide thin films were obtained by oxidizing the metallic Cu films deposited on glass substrates by e-beam evaporation. It is demonstrated that the cubic Cu phase of the as-deposited films changes into single cubic  $\text{Cu}_2\text{O}$  phase and single monoclinic  $\text{CuO}$  phase, depending on the annealing conditions. The crystallite size calculated from the XRD data is varied between 12 and  $31\text{ nm}$ . The lattice parameter ( $a$ ) is estimated to be  $\sim 3.60\text{ \AA}$  for single Cu phase and it is  $\sim 4.26\text{ \AA}$  for the single  $\text{Cu}_2\text{O}$  phase. The films with  $\text{Cu}_2\text{O}$  phase showed p-type characteristics. However, a relatively poor crystallinity of these films may have presumably limited the p-type characteristics. The films with Cu and  $\text{CuO}$  phases showed n-type conductivity. The activation energy calculated from the temperature dependent conductivity measurements is varied in the range of  $0.10\text{--}0.16\text{ eV}$ . The surface microstructure is varied depending on the variation in the annealing temperature. The poor transmittance of the as-deposited films ( $<1\%$ ) is increased to a maximum of  $\sim 80\%$  ( $800\text{ nm}$ ) on annealing at  $200^\circ\text{C}$ . The estimated direct allowed band gap is varied between  $1.73$  and  $2.89\text{ eV}$ . The films annealed at or above  $200^\circ\text{C}$  showed dual band gap, which needs to be studied in detail and further efforts are under progress. Further, the achieved p-type characteristics need to be

improved to make these films useful in the application of p-n junction-based devices.

**Acknowledgements** The authors VF, EE and GG thank Portuguese Ministry of Science and Technology (FCT-MCTES) for offering research grants through the fellowships SFRH/BD/38838/2007, SFRH/BPD/35055/2007, and SFRH/BD/27313/2006, respectively. This work was financed by the projects CTM/55945/2004, PTDC/EEA-ELC/64975/2006, and by IT R&D program of MKE (2006-S079-03, Smart window with transparent electronic devices) from ETRI Korea.

## References

- [1] E. M. Alkoy and P. J. Kelly, Vacuum **79**, 221 (2005).
- [2] S. C. Ray, Sol. Energy Mater. Sol. Cells **68**, 307 (2001).
- [3] L. O. Grondahl, Rev. Mod. Phys. **5**, 141 (1993).
- [4] B. P. Rai, Solar Cells **25**, 265 (1998).
- [5] A. O. Mousa, T. Akomolafe, M. J. Carter, Sol. Energy Mater. Sol. Cells **51**, 305 (1998).
- [6] J. Ghisjen, L. H. Tjeng, J. van Elp, H. Eskes, J. Westerink, G. A. Sawatzky, and M. T. Czyzyk, Phys. Rev. B **38**, 11322 (1988).
- [7] M. Nolan and S. D. Elliott, Phy. Chem. Chem. Phys. **8**, 5350 (2006).
- [8] C. Arjjit, G. Vinay, and K. Sreenivas, Rev. Adv. Mater. Sci. **4**, 75 (2003).
- [9] X. Mathew, N. R. Mathews, and P. J. Sebastian, Sol. Energy Mater. Sol. Cells **70**, 277 (2001).
- [10] T. Mahalinga, J. S. P. Chitra, J. P. Chu, H. Moon, H. J. Kwon, and Y. D. Kim, J. Mater. Sci., Mater. Electron. **17**, 519 (2006).
- [11] M. T. S. Nair, L. Guerrero, O. L. Arenas, and P. K. Nair, Appl. Surf. Sci. **150**, 143 (1999).
- [12] P. Samarakkara, M. A. Mallika Arachchi, A. S. Abeydeera, C. A. N. Fernando, A. S. Disanayake, and R. M. G. Rajapakse, Bull. Mater. Sci. **28**, 483 (2005).
- [13] K. Akimoto, S. Ishizuka, M. Yanagita, Y. Nawa, G. K. Paul, and T. Sakurai, Sol. Energy **80**, 715 (2006).
- [14] K. H. Yoon, W. J. Choi, and D. H. Kang, Thin Solid Films **372**, 250 (2003).

- [14] K. Santra, C. K. Sarker, M. K. Mukherjee, and B. Ghosh, *Thin Solid Films* **213**, 226 (1992).
- [15] A. Y. Oral, E. Mensur, M. H. Aslan, and E. Basaran, *Mater. Chem. Phys.* **83**, 140 (2004).
- [16] K. P. Muthe, J. C. Vyas, S. N. Narang, D. K. Aswal, S. K. Gupta, D. Bhattacharya, R. Pinto, G. P. Kothiyal, and S. C. Sabharwal, *Thin Solid Films* **324**, 37 (1998).
- [17] T. Maruyama, *Sol. Energy Mater. Sol. Cells* **56**, 85 (1998).
- [18] V. Figueiredo, E. Elangovan, G. Goncalves, P. Barquinha, L. Pereira, N. Franco, E. Alves, R. Martins, and E. Fortunato, *Appl. Surf. Sci.* **254**, 3949 (2008).
- [19] A. F. Trotman-Dickenson (ed.), *Comprehensive Inorganic Chemistry*, Vol. 3 (Pergamon, Oxford, 1973), pp. 16–39.
- [20] B. D. Cullity, *Elements of X-ray Diffraction* (Addison-Wesley, Massachusetts, 1956), p. 99.
- [21] S. Ishizuka, S. Kato, Y. Okamoto, T. Sakurai, K. Akimoto, N. Fujiwara, and H. Kobayashi, *Appl. Surf. Sci.* **216**, 94 (2003).
- [22] J. I. Pankove, *Optical Processes in Semiconductors* (Prentice-Hall, NJ, 1971), p. 34.
- [23] G. Gonçalves, E. Elangovan, P. Barquinha, L. Pereira, R. Martins, and E. Fortunato, *Thin Solid Films* **515**, 8562 (2007).
- [24] A. U. Mane and S. A. Shivashankar, *J. Cryst. Growth* **254**, 368 (2003).